International Journal of Engineering and Technology Innovation, vol. 12, no. 3, 2022, pp. 195-206

A Novel Engine Start Mechanism for an Electrified Powertrain

Neeraj Shidore, Madhusudan Raghavan*

General Motors Research and Development, Warren, USA

Received 18 December 2021; received in revised form 15 May 2022; accepted 16 May 2022

DOI: https://doi.org/10.46604/ijeti.2022.9118

Abstract

This study aims to evaluate a novel starting mechanism (planetary starter) to crank the engine of a hybrid electric vehicle for a flying start maneuver. The study describes the P2 architecture and the planetary starter mechanism. The disturbance during engine crank and driveline engagement is a vital drive quality metric for a P2 vehicle. A linear quadratic Gaussian (LQG) controller is developed to reject the disturbance. The main results of the vehicle acceleration (disturbance) with and without the controller are compared. The results indicate that the planetary starter can crank the engine, and the closed-loop controller can effectively reject the active disturbances during the engine crank event.

Keywords: P2 hybrid, tip-in, flying start, planetary starter

1. Introduction

Hybrid electric vehicles enable substantial reductions in vehicle fuel consumption (over a conventional or non-hybrid vehicle) by combining electrical energy supplied by a battery/electric motor(s) with the fuel energy supplied by an internal combustion (IC) engine [1]. Fig. 1 below depicts the typical powertrain architecture of a "P2" hybrid powertrain, wherein the electric motor is typically located in between the engine and the transmission. The "starter" (traditional pinion starter [2]) or the belt alternator starter (BAS) [3], shown in Fig. 1 are devices that are typically used to crank the engine and quickly get it started when it is needed to provide traction power. Fig. 2 below shows a typical drive profile for a P2 hybrid electric vehicle. During the constant speed or low acceleration portions, the electric motor/battery has sufficient power to meet the traction requirements; the engine is off and disconnected from the driveline (e.g., between 530 and 545 sec).

For a sudden tip-in by the driver, the engine is restarted and engaged with the driveline (clutch C1 is closed). These events are depicted as "Tip-in at Coasting" and 'Tip-in at Regen" in Fig. 2. The time it takes for the engine to crank and the clutch to close is an important metric in P2 drive quality, and is referred to as the "tip-in" response.

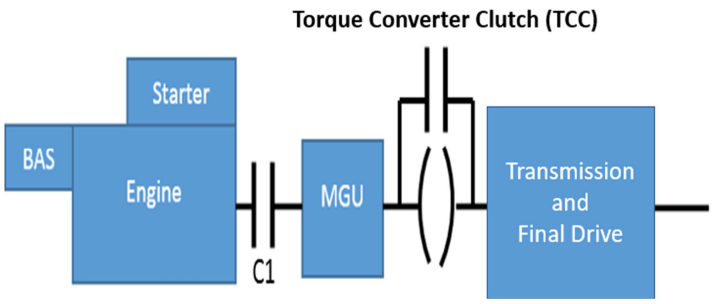

Fig. 1 Typical P2 automatic transmission powertrain architecture

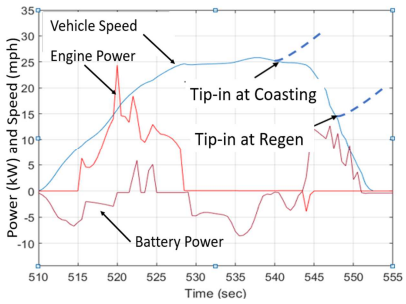

Fig. 2 Potential tip-in scenarios during electric vehicle (EV) driving

* Corresponding author. E-mail address: Madhu.raghavan@gm.com
Tel.: +1-248-9305248

A novel engine crank mechanism, called the planetary starter, is introduced in this study. As stated earlier, a tip-in manuver is an important drive quality metric for a P2. The ability of the planetary starter, to execute an engine crank and seamlessly engage it with the driveline, is evaluated using dynamic simulation. A closed-loop and model-based linear quadratic Gaussian (LQG) controller is also developed to minimize the jerk to the driveline during the crank event. This work presents the formulation of the closed-loop controller.

2. Literature Review

Some prior work in this space is as follows. Raghavan et al. [4] describes a new engine start mechanism concept that can change its operating state between two modes involving a geared or belted connection to the crankshaft. Fulks et al. [5] presents a high-performance stop-start system with a 14 Volt BAS. Ganesan et al. [6] discusses methods to enhance starter brush life for micro-hybrid (start/stop) applications. Myszka et al. [7] elaborates upon a spring-based starter system for automotive engines. Hao et al. [8] use a high-density starter to enhance engine starting performance. Raghavan [9] explains advanced starter systems for sailing/coasting operation for the European driving cycle. Wang et al. [10] use a modular triple three-phase permanent magnet starter-generator to bring improved reliability and fail-safe operation to an aircraft engine application.

Gibbs et al. [11] describes general motors' BAS system's onboard high voltage battery to supplement a low state of charge on the 12 V battery during starting events, thereby eliminating the need for an off-vehicle 12 V power source such as a jump starter. Kelly et al. [12] focuses on balancing the need to customize the belt integrated starter generator motor for different vehicle applications against the need to maintain component commonality across design variants to minimize cost, reduce risk, and accelerate development cycles. Du et al. [13] focuses on reducing driveline vibration during a diesel engine start by computing the optimal speed trajectory for minimum disturbance. Raghavan [14] introduces a method for transmission length reduction to potentially make room for electrification components of the type described in the present work.

The remainder of the work is laid out as follows: The following section describes the planetary starter mechanism and operation in detail. AMESIM software is used to evaluate the planetary starter mechanism. The following section reviews the dynamic model of the P2 in AMESIM, and key drivetrain parameters are listed. To evaluate the planetary starter, the choice of the tip-in scenario is then discussed. To achieve a quick and smooth start, closed-loop and model-based control is used to control different actuators of the planetary starter. An overview of the control methodology is provided. The study then provides simulation results of the planetary starter, followed by a summary and concluding remarks.

3. Planetary Starter Architecture

Fig. 3 below shows the architecture of the proposed planetary starter mechanism. As shown in Fig. 3, a planetary gear is inserted between the engine and the P2 motor (motor generator unit (MGU)). The engine is connected to the carrier of the planetary gear set. One end of the P2 motor is connected to the sun gear of the planetary, and the other end is connected to the torque converter. The ring gear is connected to a brake (B). The locking clutch C, nominally connecting the ring gear and the carrier, could instead be between any two members of the planetary. Table 1 below summarizes the modes of operation for the planetary starter.

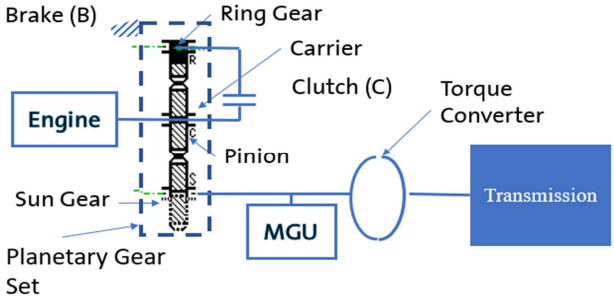

Fig. 3 Planetary starter architecture

Table 1 Planetary starter modes of operation

State	Brake B	Clutch C
EV driving	Open	Open
Engine crank	Close	Open
Engine / hybrid driving	Open	Close

Fig. 4 below shows different modes of operation for the planetary starter during an engine crank event. In the EV mode of operation, the MGU provides torque to the wheels through an open or closed torque converter, and the engine/carrier speed is zero (green, left Y-axis). When there is a need to crank the engine, at 43.03 sec, the brake B is engaged (pink, right Y-axis in pink, (%)). Brake engagement causes the carrier/engine to spin up. As soon as the engine reaches firing speed (around 350 RPM) and has completed 2 complete revolutions, the engine is fired (spark/fuel), and brake B is released. Fuel energy accelerates the engine/carrier speed to match the MGU/sun gear (blue, left Y-axis) speed. The throttle command is shown in Fig. 4 in black. The clutch C (cyan) is closed when the carrier/engine speed matches the ring speed. Closing the clutch C connects the engine with a 1:1 gear ratio to the driveline. The engine can then be used to drive the powertrain in hybrid or engine-only mode, like any other hybrid vehicle. Opening the C clutch would effectively bring the engine speed down to zero. For an excellent tip-in response, quick and smooth engagement of the engine to the driveline is critical. In that sense, for the planetary starter, three things are essential:

(1) Fast actuation of the brake decreases the ring gear speed to raise the carrier/engine speed to firing speed.

(2) Engine speed is controlled to raise the engine speed from firing speed to match the speed of the driveline, i.e., sun gear or motor speed, within the shortest possible time.

(3) Clutch C is actuated to engage the engine to the driveline, without causing any disturbance.

When comparing the planetary starter to the pinion starter/BAS starter described earlier, one can see that there is no need for an additional electrical machine (apart from the P2). However, an additional planetary gear and brake or clutch actuation for the ring gear is needed. This addition would add cost, packaging, and actuation complexity. A distinct advantage of the planetary starter over the bump start (the inertia start, wherein the vehicle inertia is used to start the engine) is that the clutch C does not have to synchronize the engine speed to the driveline speed. Instead, the clutch C can be engaged quickly once the engine and driveline speeds are close. Also, the planetary gear reduces the torque transient seen by the driveline when cranking the engine. The novelty of the planetary starter can be summarized by the fact that with this arrangement, there is no need to carry an additional electrical machine (starter or BAS) onboard the vehicle to crank the engine. Lower parts count (one less motor) can save the manufacturing cost and reduce the warranty and repair costs to the consumers due to a reduction in parts count.

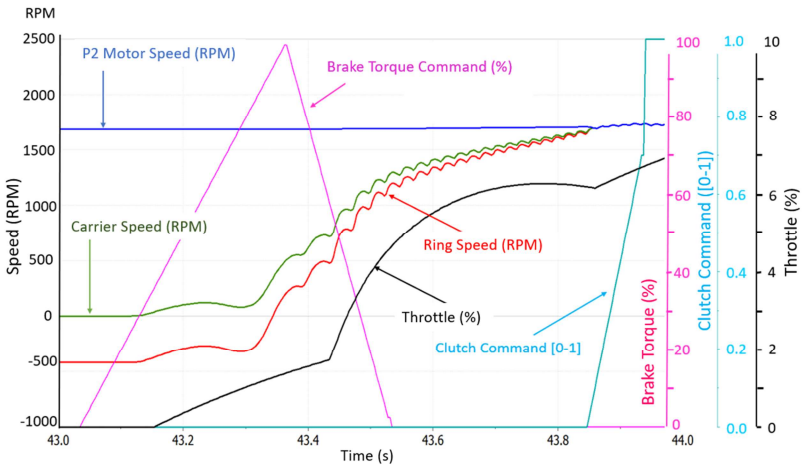

Fig. 4 Speed of planetary gear elements during an engine crank

In addition, this work shows that closed-loop control can be effectively utilized to make this novel mechanism meet drive quality requirements for an engine crank event due to the change of mind maneuver. A tip-in event is simulated in AMESIM with controls of the brake, engine, and clutch modeled in Simulink to evaluate the planetary starter concept. The following section describes the plant model in detail.

4. Modeling of a Powertrain with the Planetary Starter in AMESIM

Fig. 5 below shows the plant model in AMESIM. The planetary gear set is shown in the blue box. All the essential elements from the drivetrain perspective are red, and the engine and the planetary gearset are black. The engine model consists of an inertia element and torsional torque, which is a function of throttle and engine speed. Separate tables are used for the motoring and firing sections of the engine torque torsional pulses. The ring gear is connected to a source of brake torque, and the sun gear is connected to the rest of the powertrain to its right in the figure. The carrier is connected to the engine, and engine friction to its left.

The AMESIM model in Fig. 5 below is used as the "plant", and all the time axis plots (e.g., Fig. 4 above) are plots derived from signals measured in the AMESIM model. The case study or scenario, which illustrates the operation of the planetary starter and the closed-loop control, is described in section 5 below. The brake torque command in Fig. 4 above is commanded through the "Brake (B) Torque" input in Fig. 5 below. The throttle (%) command is "EngThrtlCmd" in Fig. 5, and the clutch command in blue in Fig. 4 above is commanded through the "Clutch (C) Comm" below. The P2 motor command, used for the EV mode operation to cancel the jerk during the actuation, is controlled through the "P2 Motor Torque" input in Fig. 5 below.

All the powertrain elements are labeled. Motor and torque converter pump inertia are lumped together (Jmot+pump). Similarly, the torque converter turbine, prop-shaft, and transmission inertia (reflected in the transmission input) are lumped together. (I_t*If) represents the gear reduction of the transmission and the final drive together. Vehicle mass and wheel inertia are lumped together. Road load (as a function of speed) is modeled as a torque source. Engine speed (w_eng), motor speed (w_mot), and vehicle speed (Vveh) are the three sensors that are used in control. Each feedback signal is delayed through a zero-order hold to emulate actual sensors in a vehicle, and white noise is added to each measurement. Kd and Cd represent the stiffness and damping of the torque converter damper. K and C represent the equivalent stiffness and damping of the prop shaft and axle.

Table 2 lists the different parameters used in the model. The transient maneuvers modeled in the following are on a mid-size sports utility veihcle (SUV). Some representative parameter values are included in Table 2. These simulations are not specific to any driving cycle.

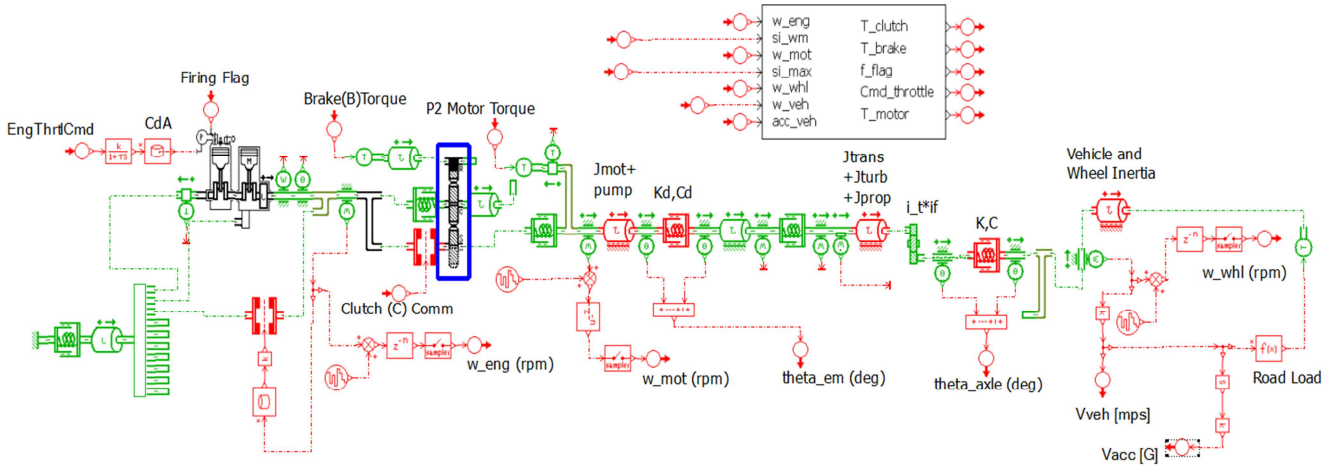

Fig. 5 Model of a P2 hybrid powertrain with planetary starter, in AMESIM

Table 2 Drivetrain parameters for the plant model in AMESIM

Parameter variable name	Parameter explanation	Value and unit
Ns	# Teeth on the sun gear	20
Nr	# Teeth on the ring gear	80
I_f	Final drive gear ratio	3.25
I_t	Second gear ratio	3.0
K	Axle and prop shaft stiffness	600 Nm/deg
C	Axle and prop shaft damping	0.75 Nm/deg/s
Je	Equivalent engine inertia	0.2 kg m^2
rw	Wheel radius	0.325 m
Bv	Vehicle viscous damping	$0.5 \times rw^2$ Nm/rad/s
M	Vehicle mass	3000 kg
rho	Air density	1.16 kg/m^3
Mu_roll	Rolling resistance coeff	0.08
Cw	Drag coefficient	0.36
Av	Frontal area	3.0 m^2
Jw	Wheel inertia	0.3 kgm^2
Jv	Equivalent vehicle inertia	$2 \times Jw + M \times rw^2 = 310$ kgm^2
Kd	Torque converter clutch (TCC) damper stiffness	22 Nm/deg
Cd	TCC damper damping	0.03 Nm/deg/sec
Jm	Motor inertia	0.05 kgm^2
Jp	TC pump inertia	0.15 kgm^2
Jtu	TC turbine inertia	0.02 kgm^2
Jtr	Transmission inertia (the 2nd gear, reflected to input)	0.09 kgm^2
Jpr	Prop shaft inertia reflected to trans input in the 2nd gear	0.03 kgm^2

5. Vehicle Scenario to Simulate the Planetary Starter Functionality and the Open-Loop Simulation Results

For a P2 architecture, an excellent tip-in response has two aspects:

(1) Rapid torque delivery to the driveline (from the MGU and the engine) is commensurate with the driver's pedal request.

(2) The engine's smooth engagement/disengagement to the driveline is without noticeable jerk or oscillations.

The driver is most sensitive to driveline disturbance (jerk/oscillations) during engine engagement at low speed, low gear, and moderate to low vehicle acceleration. In such cases, for a lousy disturbance, the magnitude of the acceleration jerk due to the disturbance may be comparable to the magnitude of the desired acceleration on tip-in. For a wide-open throttle tip-in, the quality of engagement disturbance is secondary to get a rapid and robust vehicle acceleration response. Also, the tip-in disturbance can be hidden by the significantly substantial change in acceleration due to the aggressive maneuver.

Therefore, the following scenario is chosen as a case study to evaluate the planetary starter mechanism and the closed-loop control that follows. Vehicle speed is 6 meters per second (21 kph or 13 mph), and the vehicle is operating in EV mode in the 2nd gear. In the 2nd gear, the torque converter clutch is ordinarily open. However, for this scenario, the torque converter clutch is closed. Any jerk along the driveline (due to the start mechanism) can be felt in the wheel acceleration and is not filtered by the hydrodynamic torque transfer through an open torque converter. From a drive quality perspective, the case chosen to evaluate the planetary starter and the closed-loop control is one of the extreme scenarios. Fig. 6 shows the vehicle speed and acceleration for a moderate tip-in, where the engine is reconnected to the driveline, with the planetary starter and no closed-loop control.

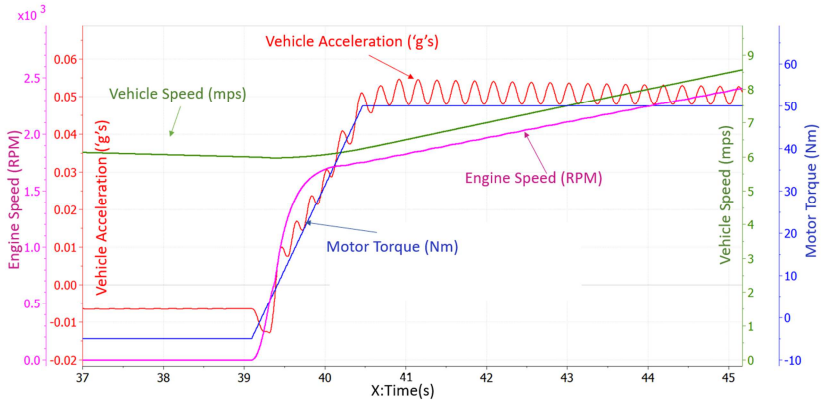

Fig. 6 Vehicle acceleration, speed, engine speed, and motor torque for a moderate tip-in

In Fig. 6 above, at around 39 seconds, there is a tip-in. Motor torque (blue, with blue Y-axis) increases immediately. The engine speed (pink, with pink Y-axis; zero before the tip-in) increases, with the engine being cranked, as explained in Fig. 4 above. Vehicle speed (green, green Y-axis), which decreases before 39 seconds, increases. Commensurate to the vehicle speed increase, the vehicle acceleration (red, red Y-axis) increases from negative to positive. Before the tip-in, i.e., before 39 seconds, the negative acceleration indicates that the vehicle is braking or coasting. Notice that vehicle acceleration is constant after about 40.5 seconds (reaches steady state) with a high-frequency ripple on it. Some noteworthy points about the acceleration behavior after the tip-in (after 39 seconds) are as follows:

(1) Despite the increase in motor torque, there is a further decrease in acceleration (around 39.2 seconds, in a notch) before the acceleration starts increasing.

(2) There is an oscillatory behavior in the acceleration throughout the increase in acceleration and even after reaching a steady state.

These behaviors are undesirable to the driver and would be perceived as a disturbance and negatively affect the drive quality metric. The three actuator signals (throttle, brake B, clutch C) that participate in cranking the engine can explain the origin of the disturbances. Fig. 7 below plots the three actuator signals (along with vehicle acceleration, engine speed, and MGU speed) for the same simulation as Fig. 6. As explained in Fig. 4, the brake command (dark blue) is used to crank the engine. The brake torque is reflected through the planetary gears and results in the initial negative acceleration event (red line, red Y-axis) around 39.3 seconds. For the engine to reach the MGU speed (green, black Y-axis), the engine throttle (black) has a significant surge as soon as the engine has reached firing speed (purple, black Y-axis) and completed 2 revolutions. This surge in engine throttle accelerates the engine to match the MGU speed as fast as possible. Finally, the throttle returns to a low value as the engine speed matches the MGU speed. Clutch C (cyan, Y-axis) closes when the engine and MGU speed match. After the clutch is closed, the throttle increases to provide engine torque to the driveline. Apart from the initial negative acceleration caused by the quick actuation of the brake, the throttle (to increase engine speed) acts as an impulse input to the system.

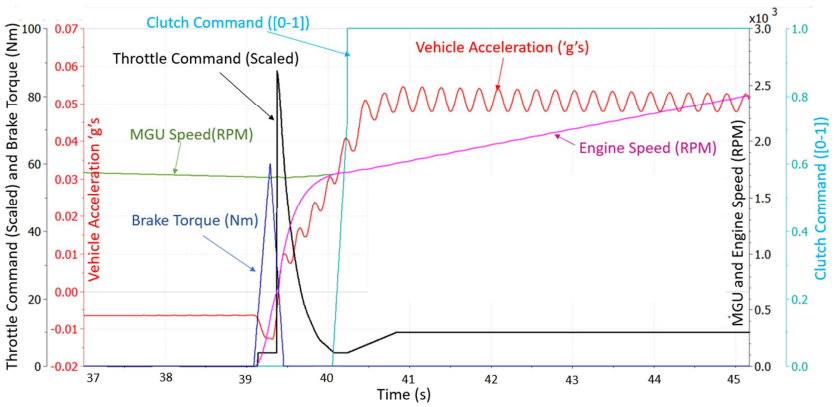

Fig. 7 Brake, clutch, and throttle command signals with vehicle acceleration, MGU, and engine speed

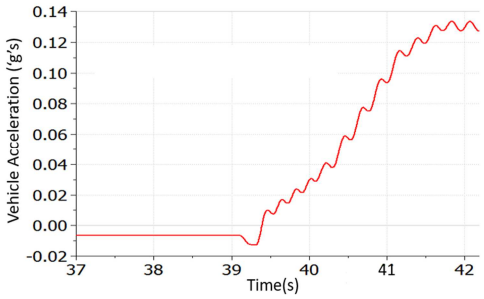

Fig. 8 Vehicle acceleration for a hard tip-in

As in Fig. 5, it is typical for driveline components to be represented in the form of inertias, dampers, and spring elements, which reflect the inertia, friction, and stiffness of different shafts and other rotating elements on the driveline. In addition to the two impulse inputs, i.e., the throttle and the brake, there is an additional step input in the form of the clutch. As shown in Fig. 7 above, impulse inputs can excite a particular resonance frequency in the driveline. This resonance, caused by the combination of the many spring/inertia and damper systems in the driveline, manifests itself as undamped oscillations of a higher frequency, as seen in Fig. 7. A pole-zero map of the state space system of the model shows a pole around 5 Hz, which is the frequency of the oscillation. Typically, such resonance can be dealt with in two ways – isolating and redesigning the section of the driveline which causes the oscillations (i.e., changing the inertia or stiffness) or removing the source of the disturbance by varying the nature of the actuation.

Fig. 8 shows the same for an aggressive tip-in. The vehicle model is maintained in the 2nd gear as a worst-case scenario. Notice that the initial jerk is due to brake B, and then the subsequent oscillations remain. The simulations shown in Figs. 6, 7, and 8 are in the 2nd gear with a locked torque converter clutch (TCC). Typically, in the 2nd gear, the TCC is open. Therefore, the torque converter naturally dampens some of the oscillations. Nonetheless, it can be argued that in the 3rd gear and at higher gears, when the TCC is locked, the oscillations and the initial jerk will still show up since the actuation mechanisms have not changed. The scenario in Figs. 6 and 7 also provides a most challenging scenario from a control perspective, with the maximum amplification of the disturbances. Indeed, if it can be shown that the above oscillations can be canceled effectively by the motor without significant energy/power loss, then at higher gears or an open TCC, the motor effort will be even lower. This would indicate that the planetary starter is a feasible starting option for a P2 hybrid, even a mild P2 hybrid.

6. Closed-Loop Control Realization for Jerk Minimization

An LQG [15] controller is developed to use motor torque to reject the disturbance associated with engine cranking caused by the brake actuation and the clutch. A Kalman filter is created to estimate some states of the system. Linear state feedback (LQR) with feedforward control is used to control the jerk.

From the AMESIM model (Fig. 5), it can be deduced that the system has six states:

$x_1 = engine\ speed.$
$x_2 = motor\ speed.$
$x_3 = turbine\ speed.$
$x_4 = wheel\ speed.$
$x_5 = (angle)\ between\ motor\ and\ turbine, i.e., due\ to\ the\ spring\ with\ stiffness\ Kd.$
$x_6 = (angle)\ between\ turbine\ and\ wheel\ inertias, i.e., due\ to\ the\ spring\ with\ stiffness\ K.$

The variables used for the physical parameters (in the following equations) are from Table 2 above. There are two modes of operation. As noted above, when clutch C is open, the plant model has 6 states. When clutch C is closed, the engine speed is the same as the motor speed, so that states x_1 and x_2 are the same. Hence, with C closed, the plant is a 5th-order system.

The control objective is to control the motor torque to reject disturbances caused by the engine (throttle), brake, and clutch. In addition, the resistance associated with aero drag and tire friction is modeled as a disturbance input (T_L). Since this is a disturbance (and not control) input to the plant, the non-linearity associated with aero drag is modeled accurately in the AMESIM plant model but not in the controller.

The dynamics of the system can be modeled in the standard state-space format in continuous time, as in Eq. (1) below:

$$\dot{X}(t) = A_O X(t) + B_O U(t) + B_{OW} W(t) \tag{1}$$

$$y(t) = C_o X(t) + v(t) \tag{2}$$

where the subscript "o" is for open, i.e., clutch C is open. $X(t)$ is the state vector of 6 elements stated earlier. $v(t)$ is sensor noise. $W(t)$ are all the plant disturbance inputs. $U(t)$ is the motor torque (control input). Wheel acceleration (x_4) is considered as the output, i.e., $y(t)$.

$$W(t) = [T_e \; T_l \; T_b \; T_c]^T \tag{3}$$

where T_e is the engine torque, T_l is the load (vehicle drag, aero) torque, T_b is the brake (B) torque, and T_c is the clutch torque. Similar equations can be defined for the system when the clutch C is closed, for a 5th-order system. The equations are not stated explicitly here to maintain the brevity of the article.

For the above Eqs. (1) and (2), the A_o, B_o, B_{ow}, and C_o matrices can be derived by inspecting the plant model in AMESIM.

$$A_o = \begin{bmatrix} \frac{-f}{J_e} & 0 & 0 & 0 & 0 & 0 \\ 0 & \frac{-C_d}{J_{mp}} & \frac{C_d}{J_{mp}} & 0 & \frac{-K_d}{J_{mp}} & 0 \\ 0 & \frac{C_d}{J_t} & \frac{-C_d}{J_t} - \frac{\mu_3{}^2 C}{J_t} & \frac{\mu_3 C}{J_t} & \frac{K_d}{J_t} & \frac{-\mu_3 K}{J_t} \\ 0 & 0 & C\frac{\mu_3}{J_v} & \frac{-C}{J_v} - \frac{B_v}{J_v} & 0 & \frac{K}{J_v} \\ 0 & 1 & -1 & 0 & 0 & 0 \\ 0 & 0 & \mu_3 & -1 & 0 & 0 \end{bmatrix} \tag{4}$$

$$B_o = \begin{bmatrix} 0 & \frac{1}{J_{mp}} & 0 & 0 & 0 & 0 \end{bmatrix}^T \tag{5}$$

$$B_{ow} = \begin{bmatrix} \frac{-1}{J_e} & 0 & \frac{1}{\mu_1 J_e} & 0 \\ 0 & 0 & \frac{-1}{J_{mp}.\mu_1.\mu_2} & \frac{-1}{J_{mp}} \\ 0 & 0 & 0 & 0 \\ 0 & \frac{-1}{J_v} & 0 & 0 \\ 0 & 0 & 0 & 0 \\ 0 & 0 & 0 & 0 \end{bmatrix} \tag{6}$$

$$C_o = \begin{bmatrix} 0 & 0 & \frac{C\mu_3}{J_v} & \frac{-C}{J_v} - \frac{B_v}{J_v} & 0 & \frac{K}{J_v} \end{bmatrix} \tag{7}$$

A, B, B_{ow}, and C are the state, control input, disturbance input, and output matrices. The suffix "o" is used to denote that the clutch is open. Similarly, equations can be derived for the 5th-order system when clutch C is closed. The speeds (states x_1 to x_4) are measured, while states x_5 and x_6 are estimated using a Kalman filter. Switching between the open clutch and closed clutch estimator model (for the Kalman filter) is done using a switch variable (α) that switches values based on the clutch position. The use of the switch variable is shown in Eq. (15) below. In addition, the fifth-order system is suitably padded with zeros to maintain the same dimensions as the sixth-order system. The above set of equations is scaled due to the significant variation in some of the states' ranges (e.g., speed and angle) to keep the controller and observer gains within tolerable ranges. The state-space system is also discretized for implementation in a computer algorithm. Standard MATLAB commands for scaling and discretization are used. Controllability and observability are similarly checked with MATLAB commands.

The objective of the state feedback control is to minimize the disturbance during the engine crank event and reconnect the engine to the drivetrain. In that sense, the objective is to minimize vehicle acceleration rate of change, i.e., jerk. The output equation, for the open and closed clutch conditions, in the continuous-time domain is given below:

$$C_o = \begin{bmatrix} 0 & 0 & \frac{C\mu_3}{J_v} & \frac{-C}{J_v} - \frac{B_v}{J_v} & 0 & \frac{K}{J_v} \end{bmatrix} \tag{8}$$

$$C_c = \begin{bmatrix} 0 & \frac{C\mu_3}{J_v} & \frac{-C}{J_v} - \frac{B_v}{J_v} & 0 & \frac{K}{J_v} \end{bmatrix} \tag{9}$$

Consider that the clutch C is open. Then, the change in wheel acceleration (state 4), in the discrete-time domain, from time step [k-1] to [k] can be given by:

$$\Delta w_4[k] = C_{o,s,d} \times W[k] - C_{o,s,d} \times W[k-1] \tag{10}$$

In the above equation, subscript "o" stands for open, "s" stands for scaled, and "d" is for the discretized version of the C matrix in Eq. (8). Similarly, W is the state vector after scaling and discretization. w_4 is the 4th state. From Eq. (10), it can be deduced that:

$$\Delta w_4[k] = C_{o,s,d} \times \Delta W[k] \tag{11}$$

As a first-order approximation, it can be stated that "jerk", i.e., the change in acceleration over a change in time, can therefore be approximated as:

$$J[k] = C_{o,s,d} \times \frac{\Delta W[k]}{\Delta T} = C_{o,s,d} \times \frac{\Delta W[k]}{T_s} \tag{12}$$

where Ts is the sampling time, and $J[k]$ is the jerk at time step [k]. Let quadratic weight matrix Q, on the discrete state vector W, be defined thus:

$$Q_{o,s,d} = \varrho.(\frac{C_{o,s,d}}{T_s})^T (\frac{C_{o,s,d}}{T_s}) \tag{13}$$

where ϱ is a scalar scaling factor. Then, the cost function ($\Im$) takes on the standard quadratic form:

$$\Im = \frac{1}{2} \sum \Delta W^T Q_{o,s,d} \Delta W + \Delta U^T R \Delta U \tag{14}$$

where R is the suitable weight on the incremental input (motor torque) ΔU. Therefore, if the LQR control is implemented in the incremental form [16], (i.e., incremental state and input ΔW and ΔU) instead of W and U, jerk is readily incorporated into the cost function as shown in Eq. (14) above and the feedback control law for motor torque, in the state feedback format, is:

$$\Delta U_{fb} = -[\alpha \times K_{o,s,d} + (1-\alpha) \times K_{c,s,d}] \times \Delta W \tag{15}$$

where $K_{o,s,d}$ are the state feedback gains when clutch C is open, i.e., $\alpha = 1$ for the scaled and discrete state vector ΔW. $K_{c,s,d}$ are the state feedback gains when clutch C is closed, i.e., $\alpha = 0$ for the scaled and discrete state vector ΔW. ΔU_{fb} is the incremental motor torque command based on feedback (*fb*). α is the switch variable as described earlier.

The feedback gains and the Kalman filter gains are calculated using standard MATLAB functions. For this controller, the brake torque is a disturbance to the system (Eq. (3)) above. This disturbance is modeled and used in feedforward control. Eq. (15) is therefore modified to:

$$\Delta U[k] = -[\alpha \times K_{o,s,d} + (1-\alpha) \times K_{c,s,d}] \times \Delta W - K_{ff} \times \Delta \widehat{T_b} \tag{16}$$

where K_{ff} is the feedforward gain, and $\widehat{T_b}$ is the estimated brake torque. ΔU is the incremental command to the motor. In the final realization, this incremental command is added to the command at the previous time step $U[k-1]$ to generate the total command $U[k]$ to the motor. The Kalman filter, feedback, and feedforward code are embedded in s Simulink m-function, which is triggered every 6.25 msec, i.e., the time step used to discretize the state matrices above.

7. Simulation Results with Closed-Loop Control for Jerk Minimization

Developing the optimal controller is to calculate the minimum motor power required to effectively cancel the jerk during the engine crank event and demonstrate the feasibility of this cranking mechanism for mild hybrids. Since some of the motor torque is "reserved" to cancel the jerk, it cannot be used for traction when the engine is cranked. Fig. 9 below shows the vehicle acceleration response with and without the LQG control (green and red lines, respectively). The disturbance during an engine cranking event due to the brake, the throttle, and the clutch disturbance inputs is much reduced. After vehicle acceleration has reached a steady value, the "ringing" effect seen with the vehicle acceleration is eliminated.

As stated earlier, the closed-loop control effort aims to reject the disturbance caused during engine cranking. Therefore, in Fig. 9, the vehicle acceleration, after tip-in, is not necessarily faster or quicker but smother. Since the tip-in response metric commonly used to judge a smooth start is a combination of quick and smooth response, the tip-in metric would improve on this account. While the focus of the closed-loop control is to remove the disturbances due to the actuation mechanism, it is equally important to make sure that the engagement of the C1 clutch to the driveline is not delayed due to the closed-loop control. Any such delay would cause the driver to feel a sense of "power loss" and would negatively impact the tip-in response score. It can be seen in Fig. 10 below that the engine speed matches the driveline within 500 msec, and the clutch C is completely closed in 700 msec. Therefore, the engine can provide torque to the driveline in about 700 msec from the start of the engine cranking event. Fig. 10 shows that the closed-loop control is working with nominally feasible times for engine engagement; actuator control is not slowed down to reduce jerk or disturbance. Thus, as seen in Figs. 9 and 10, the planetary starter provides a fast and smooth engine cranking/engine start event for the P2 hybrid, with the closed-loop control.

An important metric for the feasibility of the planetary starter concept is the additional motor power needed to cancel the disturbance. In a sense, this is the motor power reserve that must be maintained, during EV driving, so that the engine can be cranked with minimal discomfort to the driver. Any motor power, which is not used for traction, would impact the EV envelope of operation and reduce the fuel economy benefits of the hybrid technology. As stated in the earlier section, the scenario considered to evaluate the planetary starter – locked TCC in second gear, with moderate tip-in, could be considered an extreme scenario for disturbance rejection, since the 2nd gear ensures significant amplification of the disturbance, as compared to higher gears. Also, moderate tip-in ensures that the disturbance is not an order of magnitude smaller than the vehicle acceleration.

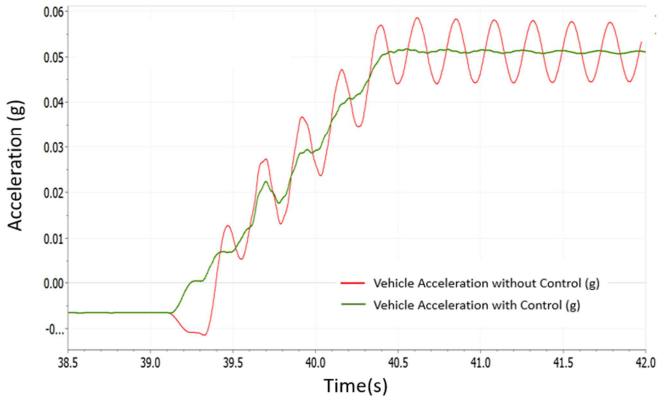

Fig. 9 Vehicle acceleration response with and without closed-loop control

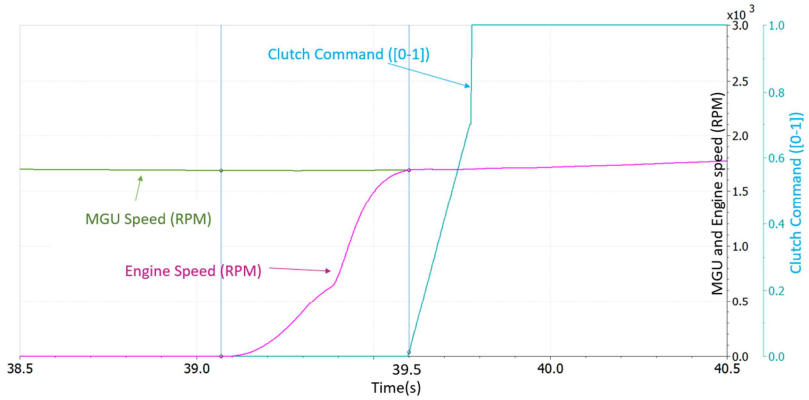

Fig. 10 Time for engagement of the engine and clutch

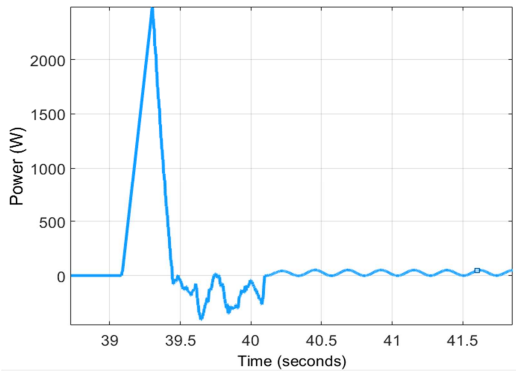

Fig. 11 Motor power demand difference between closed-loop control and no control scenarios

Fig. 11 shows the difference in motor power demand during the engine cranking maneuver, with and without the closed-loop control. As can be seen from the figure, a maximum of 2.5 kW of motor power is required to maintain a smooth tip-in response and can be primarily attributed to the initial jerk due to the brake torque. The maximum motor torque is dictated by the initial brake actuation and is therefore independent of vehicle state (i.e., vehicle speed and acceleration) but depends on the gear ratio. This value is deterministic, and 2.5 kW may represent the worst-case scenario unless a flying start maneuver with TCC locked is attempted in the first gear.

The value of the additional motor torque depends on the planetary gear ratio and the time to crank the engine. In order to ensure a smooth start, it is required that 2.5 kW of motor power be reserverd to cancel the crank jerk. Thererfore, as the motor power (used for traction) in EV mode approaches this 2.5 kW reserve, the engine should be cranked.

8. Summary and Concluding Remarks

The study presents a novel mechanism for a P2 hybrid application to crank the engine. This mechanism consists of a planetary gear set with a brake and clutch. The study gives an overview of the P2 architecture and the “flying start” maneuver,

followed by a detailed description of the planetary starter mechanism. A detailed driveline model of the P2 hybrid with the planetary starter mechanism is presented. During the flying start maneuver, the disturbance of the engine start event is a critical factor in the overall drive quality metric for a P2 hybrid vehicle. With closed-loop control, simulation results show the planetary starter's use during a flying start mechanism, with satisfactory drive quality.

In addition, it can be noted that the planetary gear ratio heavily influences the motor torque required for jerk minimization. In this work, a ratio of 4 is assumed. Furthermore, certain simplification is assumed for control development, for example - no gear lash during the transition from negative to positive torque. Also, instantaneous motor torque delivery is assumed, due to much smaller electrical time constants of the electric machine. The simulation results presented in this study need to be validated with hardware tests.

Conflicts of Interest

The authors declare no conflicts of interest.

References

[1] N. Shidore, et al., "Fuel Economy and Drivability Trade-Off for Mild Hybrid Electric Vehicle Architectures," Industrial Problems on Machines and Mechanisms (IPRoMM), pp. 709-719, December 2020.
[2] L. Hao, et al., "Brushless Fast Starter for Automotive Engine Start/Stop Application," IEEE Transactions on Industry Applications, vol. 56, no. 6, pp. 6041-6052, November-December 2020.
[3] W. Cai, "Comparison and Review of Electric Machines for Integrated Starter Alternator Applications," Conference Record of the IEEE Industry Applications Conference, pp. 386-393, October 2004.
[4] M. Raghavan, et al., "The Kinematics and Dynamics of Engine Start Systems," Asian Mechanism and Machine Science (Asian MMS), pp. 293-302, December 2018.
[5] G. Fulks, et al., "High Performance Stop-Start System with 14 Volt Belt Alternator Starter," SAE International Journal of Engines, vol. 5, no. 3, pp. 864-873, August 2012.
[6] B. K. Ganesan, et al., "Enhancement of Starter Brush Life for Micro Hybrid (Start/Stop) Applications," International Conference on Advances in Design, Materials, Manufacturing, and Surface Engineering for Mobility, Article no. 2018-28-0102, July 2018.
[7] D. H. Myszka, et al., "Development of a Spring-Based Automotive Starter," SAE International Journal of Commercial Vehicles, vol. 7, no. 1, pp. 286-294, April 2014.
[8] L. Hao, et al., "Enhancing Engine Starting Performance Using High-Power Density Brushless Starter," WCX SAE World Congress Experience, Article no. 2020-01-0459, April 2020.
[9] M. Raghavan, "Optimizing Engine Start Systems with Application to Sailing/Coasting and Mild Hybridization," Advances in Technology Innovation, vol. 5, no. 1, pp. 1-9, January 2020.
[10] B. Wang, et al., "Design Optimization of Modular Permanent Magnet Machine with Triple Three-Phase for Aircraft Starter Generator," AeroTech Conference, Article no. 2022-01-0055, March 2022.
[11] J. Gibbs, et al., "On Board Jump Start for Belted Alternator Starter Hybrids," SAE World Congress and Exhibition, Article no. 2011-01-0867, April 2011.
[12] J. Kelly, et al., "Specification and Design of a Switched Reluctance 48V Belt Integrated Starter Generator (B-ISG) for Mild Hybrid Passenger Car Applications," SAE World Congress and Exhibition, Article no. 2014-01-1890, April 2014.
[13] L. Du, et al., "Optimal Speed Profile for Minimum Vibration during Engine Start Using Pontryagin's Minimum Principle Approach," New Energy and Intelligent Connected Vehicle Technology Conference, Article no. 2019-01-5026, November 2019.
[14] M. Raghavan, "Long Pinions for Alternative Transmission Mechanizations," Proceedings of Engineering and Technology Innovation, vol. 9, pp. 32-37, July 2018.
[15] J. B. Burl, Linear Optimal Control, H2 and H-Infinity Methods, Addison Wesley Publications, 1998.
[16] L. A. Sievers, et al., "Comparison of Two LQG-Based Methods for Disturbance Rejection," Proceedings of the IEEE Conference on Decision and Control, pp. 483-485, December 1989.